A Model-Based Strategy for Interturn Short-Circuit Fault Diagnosis in PMSM

Manuel A. Mazzoletti, *Student Member, IEEE*, Guillermo R. Bossio, *Senior Member, IEEE*, Cristian H. De Angelo, *Senior Member, IEEE*, and Diego R. Espinoza-Trejo, *Associate Member, IEEE*

***Abstract*—A model-based method for interturn short-circuit fault detection and isolation in permanent magnet synchronous machines (PMSMs) is proposed in this paper. The fault detection is realized based on a residual current vector (RCV) generated by the difference between the measured stator currents and the stator currents estimated by a state observer. In order to avoid false alarms due to possible undesired perturbations, the sequence decomposition of the RCV is performed by employing different reference-frames. Thus, the proposed RCV allows the correct detection of interturn short-circuit faults and quantification of the fault severity in any faulty stator-phase winding. Moreover, since the back-EMF generated by the magnets is proportional to the rotor shaft speed, the electrical angular speed is estimated through the stator voltages measurement, without using a speed sensor. Simulation results from the three-phase PMSM dynamic model that allows considering the interturn short-circuit fault in any stator phase-windings are presented. The proposed method is validated using a three-phase PMSM prototype with modified stator windings. The robustness and the reliability of the proposal was tested for several interturn fault conditions under transient conditions including different disturbances.**

***Index Terms*—Fault diagnosis, interturn short circuit, observer, model-based approach, permanent-magnet synchronous machines (PMSMs).**

Nomenclature

$qd0$	Variables in $qd0$ reference frame.
$\mathbf{v}_{\rm qd}$	Vector of stator voltages.
$\mathbf{i}_{\rm qd}$, $i_{\rm f}$	Vector of stator currents, fault current.
$r_{\rm s}$, $r_{\rm f}$	Stator resistance, fault resistance.
p	Operator $\frac{d}{dt}$.
$\mathbf{\Psi}_{\rm qd}$	Vector of stator fluxes.
$\mathbf{\Psi}_{\rm qd,pm}$	Fluxes of the permanent magnets.
$\boldsymbol{\mu}_{\rm qd}$	Vectorial fault factor, VFF.
$\mathbf{e}_{\rm qd}$	Vector of estimation errors.
$\Vert\cdot\Vert$	Euclidean norm.
$L_{\rm ls}$, $L_{\rm m}$	Stator leakage and magnetizing inductance.
$T_{\rm e}$	Electromagnetic torque.
ps, ns	Subscript: Positive an negative sequence.
T	Superscript: Transpose.
$\widetilde{V}$	Stator voltage phasor.
$\widetilde{E}$	Back EMF phasor.
$\widetilde{I}$, $\widetilde{I}_{\rm f}$	Stator current phasor, fault current phasor.
$\theta_{\rm r}$	Angular rotor position.
$\theta_{\rm e}$	Angular position relative to the stator axis.
$\omega_{\rm e}$	Electrical angular speed.
P	Number of pole pairs.
$\psi_{\rm pm}$	Amplitude of the permanent magnet flux.

Manuscript received September 23, 2016; revised January 5, 2017 and February 15, 2017; accepted March 10, 2017. This work was supported in part by the Consejo Nacional de Investigaciones Científicas y Técnicas, Argentina, in part by the Universidad Nacional de Río Cuarto, Argentina, and in part by the Universidad Nacional de Misiones, Argentina. *(Corresponding author: Manuel A. Mazzoletti.)*

M. A. Mazzoletti, G. R. Bossio, and C. H. De Angelo are with the Grupo de Electrónica Aplicada, Universidad Nacional de Río Cuarto, Río Cuarto X5804BYA, Argentina, and also with the Consejo Nacional de Investigaciones Científicas y Técnicas, Buenos Aires C1033AAJ, Argentina (e-mail: m.a.mazzoletti@ieee.org; gbossio@ing.unrc.edu.ar; cdeangelo@ieee.org).

D. R. Espinoza-Trejo is with the Department of Mechatronics Engineering, Coordinación Académica Región Altiplano, Universidad Autónoma de San Luis Potosí, San Luis Potosí 78700, México (e-mail: drespinozat@ieee.org).

Color versions of one or more of the figures in this paper are available online at http://ieeexplore.ieee.org.

Digital Object Identifier 10.1109/TIE.2017.2688973

I. Introduction

PERMANENT-MAGNET synchronous machines (PMSMs) are massively used because of several attractive features. In PMSMs, the magnetic flux induced in the stator windings is generated by rare-earth magnets (e.g., NdFeB or SmCo, among others) located on the rotor [1]. Unlike the ferrite or AlNiCo magnets, rare-earth magnets improves the magnetic flux density and consequently the efficiency and power density also increases. Because of this, PMSMs are used in several applications that require high efficiency and a precise torque control under different operating conditions.

Insulation of the stator windings is the major source of failures in electrical machines [2]. The progressive degradation of the insulation may cause short circuit between the turns producing a overheat into the stator winding [3]. As a result, a large current flows through the shorted turns that impairs the magnetic coercivity and produces partial demagnetization of the permanent magnets due to located magnetic flux [4]. Furthermore, if temperature of the magnet exceeds the threshold of the Curie temperature, its magnetization is reduced to zero. Therefore, condition monitoring methods (CMMs) able to detect interturn short-circuit faults are essential in order to avoid catastrophic failures such as turn to ground faults, phase to phase or the irreversibly core damage [5].

Both electrical and mechanical signals measurements are used in CMM for recognizing anomalies into the electrical machines. In this context, most of the signal-based fault-detection methods proposed in the literature are based on harmonic monitoring in both the stator current or voltage in order to identify frequency components introduced by different faults [6], [7]. However, disturbances that may result from the motor drive or even due to other types of faults produce similar effects in the currents spectra [8]. Because of this, the fault identification becomes a difficult task. In order to decouple the effects of the motor drive, some of the proposed methods are based on the zero-sequence voltage component (ZSVC) harmonic monitoring [9]. A possible disadvantage of the ZSCV-based methods is that the neutral point connection of the stator windings is required and also an external resistor network is implemented for measuring the voltage component. Nonstationary operation has been considered in several CMM based on time-frequency [10], wavelet [11], Wigner Ville analysis [12], and Vold–Kalman filter [13], [14]. Most of these methods are based on selective filters to isolate the specific frequency component associated with the faults. On the other hand, there are model-based methods for fault detection which use mathematical models [15]. In this sense, several lumped-parameters mathematical-model with stator fault, both in the *abc* and *qd0* reference frames, have been developed in the literature [16]–[20]. In [21], a dynamic model with interturn short-circuit fault in one of the phase stator-winding for a three-phase induction machine (IM) is proposed. A model that considers an interturn stator fault, but in any phase winding by means of a vectorial fault factor is presented in [16]. In this case, a residual signal is generated by using a state observer, in order to detect and identify stator windings faults. In reference to PMSMs, some recent works proposed dynamic models with interturn short-circuit fault in one of the phase stator-winding for a three-phase PMSM [17]–[20]. Generally, the models proposed in the literature are analytically extensive, because of this, they become difficult to use for online applications. Furthermore, as mentioned above, the effects of interturn short-circuit faults were included in one of the stator windings, thus, such models should be modified in order to consider the fault in any other phase windings. A relevant feature regarding model-based methods is that they require the knowledge of machine parameters. Model uncertainties, parameter variations, or manufacturing imprecision of the PMSM are the main disadvantages that should be considered when analyzing the robustness and reliability of the monitoring diagnosis techniques [22]. Model-based methods also require knowing the back EMF for the online application. In some cases, fault detection is performed by comparing the reference back EMF with those estimated by state observers [23], [24]. Other methods detect the stator fault by comparing the measured currents with the estimated ones [16], [25]. The reference back EMF can be obtained by different methods. In [25], the back EMF is saved in data memory for the machine in generator mode considering operating conditions without perturbations. On the other hand, Sarikhani and Mohammed [23] calculate the reference back EMF through a model based on finite elements (FE). In all cases, n reference back EMF are required to consider the n operating conditions and the uncertainties that are not included in the estimator design or calibration stage. In addition, the position and rotor speed are measured from an external sensor.

In this paper, a model-based method for interturn short-circuit fault detection and isolation in three-phase PMSM is proposed. This method is based on the extended dynamic model in $qd0$ stationary reference-frame that allows including the interturn short-circuit fault in any phase-windings, previously validated in [26]. Stator fault detection is performed based on a residual current vector (RCV) signal generated by the difference between the stator currents measurement and the stator currents estimated by using a state observer. In order to avoid false alarms, the effects of parameter variations and also other undesired perturbations are decoupled through the sequence decomposition of the RCV signal by employing the reference-frame theory [27]. The obtained RCV allows the correct detection of the incipient interturn short-circuit fault, the complete recognition of the fault severity, and the fault isolation for any faulty stator winding. Unlike previous proposals [23], [25], the angular rotor position and the electrical angular speed are estimated online through the measurement of stator voltages to calculate the back EMF generated by the magnets; thus, the proposed method can be implemented without the use of an external sensor. Therefore, the main advantages of the method proposed in this paper are as follows:

1) a dynamic model that allows including the stator interturn short-circuit fault in any phase-windings for three-phase PMSM;
2) an RCV that allows the implementation of a single state observer for the detection and isolation of the stator windings faults instead of a bank of observers for each one of the phase windings faults;
3) angular speed is estimated by using the stator voltages measurement, avoiding the need of a position or speed sensor;
4) decoupling of the effects of undesired disturbances such as model parameter uncertainties, asymmetric stator currents, measurement noise and others, for the secure identification of the stator fault by defining a new fault severity factor.
5) correct fault diagnosis for several operating points and transient conditions.

Simulation results from the three-phase PMSM dynamic model under different fault condition are presented. Finally, for validating the proposal, experimental tests are performed using a 3/4 HP three-phase PMSM prototype with modified stator windings. The robustness and the reliability of the proposed method was tested for several interturn fault conditions even under parameter variations and external disturbances.

II. Extended PMSM Model With Interturn Short-Circuit Fault

Briefly, an interturn short-circuit fault can be modeled as an additional electrical circuit formed by the damaged turns of the stator phase windings, such as the electrical scheme of PMSM stator winding with interturn fault in phase a shown in

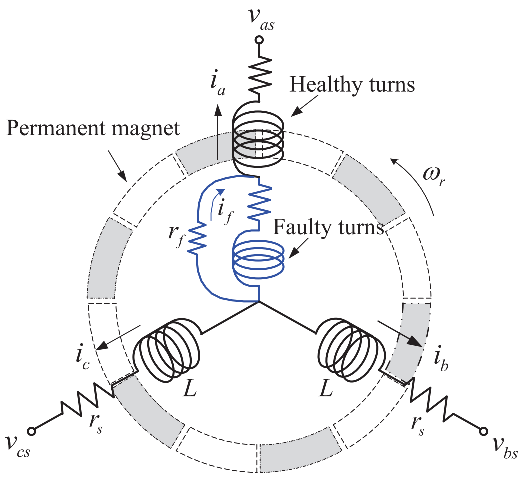

Fig. 1. Scheme of the stator winding of a PMSM with an interturn short-circuit fault in phase winding a.

Fig. 1. Additionally, the contact resistance between the shorted turns is represented by the fault resistor r_f. Meanwhile, the r_f reduction increases the fault severity since a greater fault current i_f circulates through the PMSM windings. Based on these assumptions, the extended PMSM model with stator fault is developed in the following section.

A. PMSM Model With Stator Fault in the qd0 Frame

The extended dynamic model that allows including a stator interturn fault in any phase windings is derived similar to [16], [21] for IM and to [17], [18] for PMSM. First, the dynamic model with stator fault for each phase a, b, and c are formulated. Second, the dynamic models are transformed to the *qd0* stationary reference frame. In this application, the zero sequence component is neglected since the neutral point connection is not available. Finally, an extended dynamic model is derived by introducing a vectorial fault factor (VFF). Using the dynamic model with interturn short-circuit stator fault validated in [26], this PMSM model is given by

$$\mathbf{v}_{qd} = r_s \mathbf{i}_{qd} + p\mathbf{\Psi}_{qd} - \frac{2}{3}\boldsymbol{\mu}_{qd}\left[r_s + \left(L_{ls} + \frac{3}{2}L_m\right)p\right] i_f \quad (1)$$

$$\mathbf{v}_{qd}^{\mathbf{T}}\,\boldsymbol{\mu}_{qd} = \left[\left\|\boldsymbol{\mu}_{qd}\right\|\left(1 - \frac{2}{3}\left\|\boldsymbol{\mu}_{qd}\right\|\right)\right](r_s + L_{ls}p)\, i_f + r_f i_f \quad (2)$$

where the stator flux is composed of

$$\mathbf{\Psi}_{qd} = \left(L_{ls} + \frac{3}{2}L_m\right)\mathbf{i}_{qd} + \mathbf{\Psi}_{qd,pm}. \quad (3)$$

For the formulation of (1)−(3), the following assumptions were considered: an infinite iron permeability without magnetic saturation, an uniform and constant air gap, additionally, both the distribution of the stator windings and the magnetic flux density are balanced and contain only the fundamental positive-sequence component.

Therefore, from (1), (2) the VFF is defined as follows:

$$\boldsymbol{\mu}_{qd} = \mu\left[n_q\ n_d\right]^{\mathrm{T}} \quad (4)$$

where n_q and n_d are real values $\in \mathbb{R}$. Therefore, the stator fault is completely characterized by VFF-component $\boldsymbol{\mu}_{qd} = [\mu_q \mu_d]^{\mathrm{T}}$ in *qd*-plane as follows: $\left\|\boldsymbol{\mu}_{qd}\right\|$ is the percentage of faulty turns with respect to the total turns of the complete-phase winding. $\angle\boldsymbol{\mu}_{qd}$ is the interturn fault location into stator windings.

Thus, according to the faulty phase windings, the n_q and n_d parameters can be set as $[1\ 0]^{\mathrm{T}}$ for faulty phase winding a, indicating a 0 degree angle of VFF in *qd*-plane. Similar, n_q and n_d are set as $[-\frac{1}{2}\ -\frac{\sqrt{3}}{2}]^{\mathrm{T}}$ or $[-\frac{1}{2}\ \frac{\sqrt{3}}{2}]^{\mathrm{T}}$ for faulty phase b or c, respectively. For these cases, the angle of VFF will be $\frac{2\pi}{3}$ or $\frac{4\pi}{3}$ in *qd*-plane, respectively. Note that for case $\left\|\boldsymbol{\mu}_{qd}\right\| = 0$, the first two terms on the right of (1) correspond to the healthy PMSM [27].

The electromagnetic torque is given by

$$T_e = \psi_{pm}\left(i_q \cos\theta_r - i_d \sin\theta_r - \boldsymbol{\mu}_{qd}^{\mathbf{T}}\begin{bmatrix}\cos\theta_r\\ \sin\theta_r\end{bmatrix} i_f\right). \quad (5)$$

Unlike similar models [17], [18], [25], the included VFF gives a significant advantage for the fault analysis since only two parameters must be set to change between three different dynamic models according to the faulty winding; thus, resulting in a minimum computational effort.

B. PMSM Model for Steady-State Condition

In order to implement the proposed method for interturn short-circuit fault detection and isolation, the PMSM steady-state model is obtained next. The steady-state model will allow us to precisely analyze the RCV signal. In this operating condition, a voltage source given by $v_{qd} = \widetilde{V}_{ps}e^{j\omega_e t} + \widetilde{V}_{ns}e^{-j\omega_e t}$ is applied to the extended dynamic model with stator fault. Also, assuming no significant electrical angular speed variations ω_e, the back EMF can be defined as $E_{qd} = \widetilde{E}_{ps}e^{j\omega_e t} + \widetilde{E}_{ns}e^{-j\omega_e t}$.

Therefore, similar to [16] for IM, the PMSM steady-state model with interturn short-circuit fault is given by

$$\widetilde{V}_{ps} = (r_s + j\omega_e L)\left(\widetilde{I}_{ps} - \frac{1}{3}\boldsymbol{\mu}_{qd}\widetilde{I}_f\right) + \widetilde{E}_{ps} \quad (6)$$

$$\widetilde{V}_{ns} = (r_s + j\omega_e L)\left(\widetilde{I}_{ns} - \frac{1}{3}\boldsymbol{\mu}_{qd}^{*}\widetilde{I}_f\right) + \widetilde{E}_{ns}. \quad (7)$$

Also, the additional electrical circuit formed by the damaged turns is defined by

$$\boldsymbol{\mu}_{qd}^{*}\widetilde{V}_{ps} + \boldsymbol{\mu}_{qd}\widetilde{V}_{ns} = K\left(r_s + j\omega_e L_{ls}\right)\left\|\boldsymbol{\mu}_{qd}\right\|\widetilde{I}_f + r_f\widetilde{I}_f \quad (8)$$

where $\boldsymbol{\mu}_{qd}^{*}$ is the conjugate of VFF, $L = L_{ls} + \frac{3}{2}L_m$ and $K = \left(1 - \frac{2}{3}\left\|\boldsymbol{\mu}_{qd}\right\|\right)$.

From (6)–(8), the sequence component equivalent-circuits are derived, shown in Fig. 2(a) and (b). Fig. 2(c) shows the equivalent electrical circuit for the loop formed by the short circuit between the turns (see Fig. 1). Note that for healthy PMSM [see Fig. 2(a) and (b) when $\left\|\boldsymbol{\mu}_{qd}\right\| = 0$], the equivalent-circuits represent the normal-operation of the PMSM under power supply voltage unbalance.

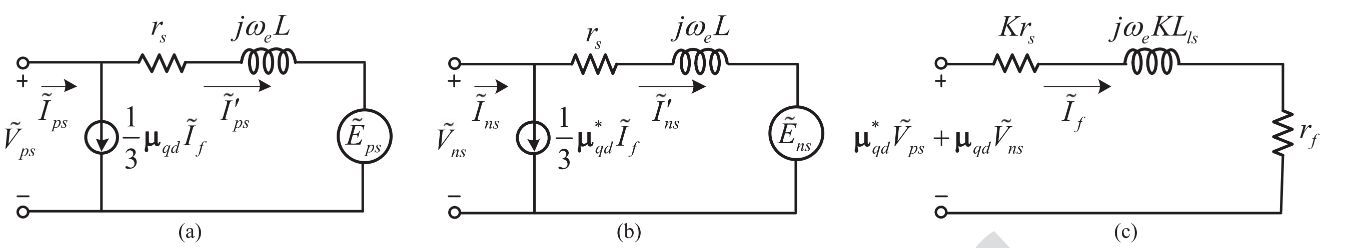

Fig. 2. Steady-state PMSM equivalent circuits with an interturn short-circuit fault. (a) Positive-sequence component. (b) Negative-sequence component. (c) Fault circuit.

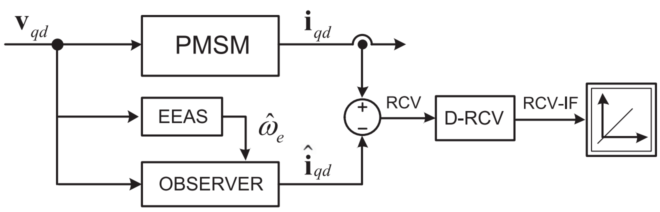

Fig. 3. Proposed scheme for the stator interturn short-circuit fault detection and isolation in PMSM.

III. Proposed Model-Based Diagnosis Method

As previously mentioned, this proposed method is based on the extended dynamic model that allows including interturn fault in any phase-windings for PMSMs. Fig. 3 shows a general scheme of the proposed stator fault detection and isolation strategy for PMSMs from the measurement of stator currents and voltages. With this aim, a state observer based on the PMSM normal-operation model is designed for estimating the stator currents from the voltages measurement. Since for obtaining the back EMF, the knowledge of the electrical angular speed ω_e is required, this variable is estimated online from the stator voltages measurement; thus avoiding the use of a speed sensor (block *Estimation of Electrical-Angular Speed*, **EEAS**). The detection of incipient faults is realized through the RCV generated by the difference between the measured stator currents and the currents estimated by the observer. However, the resulting RCV signal could be produced by other disturbances such as model parameter uncertainties, asymmetric currents, measurement noise, among others. Therefore, in order to avoid false alarms, the effects of undesired perturbations are decoupled through the sequence decomposition of the RCV by employing the reference-frame theory (block *Decomposition of Residual Current Vector*, D-RCV).

A. State Observer

In this paper, a state observer based on a normal-operation model of the PMSM is proposed to estimate stator currents. Thus, from (1) to (3), the stator currents (in *qd*-coordinates) can be defined as

$$\mathbf{i}'_{qd} = \mathbf{i}_{qd} - \frac{2}{3}\boldsymbol{\mu}_{qd} i_f. \tag{9}$$

Then, the proposed state observer is given by

$$p\hat{\mathbf{i}}'_{qd} = \frac{1}{L}\left(\mathbf{v}_{qd} - r_s \hat{\mathbf{i}}'_{qd} - \psi_{pm}\hat{\omega}_e \hat{\mathbf{E}}_{qd}\right) \tag{10}$$

where the estimated currents are defined by $\hat{\mathbf{i}}'_{qd} = [\hat{i}'_q \; \hat{i}'_d]^{\mathbf{T}}$.

The back EMF given by $\hat{\mathbf{E}}_{qd} = [\hat{E}_q \; \hat{E}_d]^{\mathbf{T}}$ will be calculated in real time by using the electrical angular speed $\hat{\omega}_e$ estimated from the voltages measurement $\mathbf{v}_{qd}$. Note that, from (10), the output voltage for no-loaded condition ($\mathbf{i}_{qd} = 0$) is directly the back EMF. In this case, angular rotor position relative to the stator axis can be determined from the measured output voltages as follows:

$$\hat{\theta}_e \approx \mathrm{atan2}\,(v_d, v_q) \tag{11}$$

where $\theta_e = \mathrm{P}\theta_r$.

On the other hand, if the PMSM is loaded ($\mathbf{i}_{qd} \neq 0$), the output voltage will be different from the back EMF due to the voltage drop in the stator resistance and inductances. However, the difference between relative position of the back EMF and the output voltage will be constant and small magnitude. Then, from (11) the rotor speed can be estimated as

$$\hat{\omega}_e\,(k) = \frac{\hat{\theta}_e\,(k) - \hat{\theta}_e\,(k-1)}{\Delta_T} \tag{12}$$

where Δ_T is the time between samples.

To eliminate the noise in the speed estimation, a low-pass filter (LPF) is used. Otherwise, to avoid the derivative, from the estimated rotor position the speed can also be calculated using high-gain observers [28].

Considering a difference between the actual and the estimated speed, the error dynamics between the measured and estimated currents for the healthy PMSM is given by

$$p\mathbf{e}_{qd} = -\frac{r_s}{L}\mathbf{e}_{qd} - (\omega_e - \hat{\omega}_e)\frac{\psi_{pm}}{L}\mathbf{E}_{qd}. \tag{13}$$

Then, if there is no speed estimation error, the estimation error of the currents will tend to zero. On the other hand, if there is a difference between the actual and estimated speed, this difference only affects the amplitude of the error term, but not the sequence of the back EMF. In other words, if the back EMF contains only the fundamental positive-sequence component, the same will occur with the current estimation error. Therefore, once the currents are estimated, the early detection of incipient stator fault is performed through the RCV given by

$$\mathbf{e}_{qd} = \mathbf{i}_{qd} - \hat{\mathbf{i}}'_{qd} = \frac{2}{3}\boldsymbol{\mu}_{qd} i_f + \mathbf{e}_p. \tag{14}$$

For a healthy PMSM, (14) should be usually zero or close to zero, but it is different from zero when a stator interturn short-circuit fault occurs. It can be seen that the first term contains information about the stator fault ($\left\|\boldsymbol{\mu}_{qd}\right\|$, $\angle\boldsymbol{\mu}_{qd}$ and i_f), while the second term $\mathbf{e}_p$ corresponds to the current error produced by the other undesirable disturbances like parameter errors or speed estimation errors, as shown in (13).

B. Analysis of the RCV

In order to calculate analytically the RCV, from (6) and (7), the stator currents phasors $\widetilde{I}_{ps}$ and $\widetilde{I}_{ns}$ are obtained as a function of $\widetilde{V}_{ps}$, $\widetilde{V}_{ns}$, and $\widetilde{I}_f$, as follows:

$$\widetilde{I}_{ps} = \frac{\widetilde{V}_{ps} - \widetilde{E}_{ps}}{Z_{ps}} + \frac{1}{3}\boldsymbol{\mu}_{qd}\widetilde{I}_f \tag{15}$$

$$\widetilde{I}_{ns} = \frac{\widetilde{V}_{ns} - \widetilde{E}_{ns}}{Z_{ns}} + \boldsymbol{\mu}^*_{qd}\widetilde{I}_f. \tag{16}$$

On the other hand, from (8), the fault current phasors are given by

$$\widetilde{I}_f = \frac{\frac{\boldsymbol{\mu}^*_{qd}}{\left\|\boldsymbol{\mu}_{qd}\right\|}\widetilde{V}_{ps} + \frac{\boldsymbol{\mu}^*_{qd}}{\left\|\boldsymbol{\mu}_{qd}\right\|}\widetilde{V}_{ns}}{\left(1 - \frac{2}{3}\left\|\boldsymbol{\mu}_{qd}\right\|\right)(r_s + j\omega_e L_{ls}) + \frac{r_f}{\left\|\boldsymbol{\mu}_{qd}\right\|}}. \tag{17}$$

By including (17) into (15)–(16), the stator currents are expressed as

$$\widetilde{I}_{ps} = \frac{\widetilde{V}_{ps} - \widetilde{E}_{ps}}{Z_{ps}} + \frac{1}{3}\left\|\boldsymbol{\mu}_{qd}\right\|\frac{\widetilde{V}_{ps}}{Z_f} + \frac{1}{3}\boldsymbol{\mu}^*_{qd}\frac{\widetilde{V}_{ns}}{Z_f} \tag{18}$$

$$\widetilde{I}_{ns} = \frac{\widetilde{V}_{ns} - \widetilde{E}_{ns}}{Z_{ns}} + \frac{1}{3}\boldsymbol{\mu}_{qd}\frac{\widetilde{V}_{ps}}{Z_f} + \frac{1}{3}\left\|\boldsymbol{\mu}_{qd}\right\|\frac{\widetilde{V}_{ns}}{Z_f} \tag{19}$$

where $Z_{ps} = Z_{ns} = Z = r_s + j\omega_e L$ is the sequence impedance and $Z_f = \left(1 - \frac{2}{3}\left\|\boldsymbol{\mu}_{qd}\right\|\right)(r_s + j\omega_e L_{ls}) + \frac{r_f}{\left\|\boldsymbol{\mu}_{qd}\right\|}$ is defined as the fault impedance.

Similarly, from normal-operation model (10), the positive- and negative-sequence components phasors of the estimated stator currents are obtained as

$$\widetilde{I}'_{ps} = \frac{\widetilde{V}_{ps} - \widetilde{E}_{ps}}{\hat{Z}} \tag{20}$$

$$\widetilde{I}'_{ns} = \frac{\widetilde{V}_{ns} - \widetilde{E}_{ns}}{\hat{Z}} \tag{21}$$

where $\hat{Z}$ is the nominal characteristic impedance.

Finally, the difference between the measured stator currents (18)–(19) and the stator currents estimated from (20)–(21), it is possible to obtain the components of RCV as follows:

$$\widetilde{e}_{Ips} = \left(\frac{1}{Z} - \frac{1}{\hat{Z}}\right)\Delta_{vps} + \frac{1}{3Z_f}\left(\left\|\boldsymbol{\mu}_{qd}\right\|\widetilde{V}_{ps} + \boldsymbol{\mu}^*_{qd}\widetilde{V}_{ns}\right) \tag{22}$$

$$\widetilde{e}_{\mathrm{Ins}} = \left(\frac{1}{Z} - \frac{1}{\hat{Z}}\right)\Delta_{vns} + \frac{1}{3Z_f}\left(\boldsymbol{\mu}_{qd}\widetilde{V}_{ps} + \left\|\boldsymbol{\mu}_{qd}\right\|\widetilde{V}_{ns}\right) \tag{23}$$

where $\Delta_{vps} = \left(\widetilde{V}_{ps} - \widetilde{E}_{ps}\right)$ and $\Delta_{vns} = \left(\widetilde{V}_{ns} - \widetilde{E}_{ns}\right)$.

From (22) and (23), the following features can be highlighted: 1) the estimation errors due to parameter variations of the state observer are related with the first term on the right side, while the other terms are produced by the stator fault; 2) both RCV-sequence components, $\widetilde{e}_{Ips}$ and $\widetilde{e}_{\mathrm{Ins}}$, depend on the positive- and negative-sequence voltages. In this case, two situations can be analyzed. First, by assuming that the PMSM parameters are accurately known, the first terms in (22) and (23) should be zero or close to zero, and thus, the sequence components of RCV are only due to the stator fault. However, the parameter errors may occur by various causes such as temperature variation, saturation, measurement error, and other perturbations and, thus, such terms can not be neglected. Then, since usually the negative-sequence voltage represents a very small percentage of the positive sequence voltage, the effect of the parametric error is more significant in the error of the positive sequence [first term in (22)] than in the error of the negative sequence [first term in (23)]. Therefore, it can be concluded that the negative-sequence of RCV $\widetilde{e}_{\mathrm{Ins}}$ can be used to detect a stator fault since it is practically independent of parametric errors. Then, by neglecting the negative-sequence voltage and considering only the fundamental of positive-sequence component of the magnetic flux, the RCV-sequence components are given by

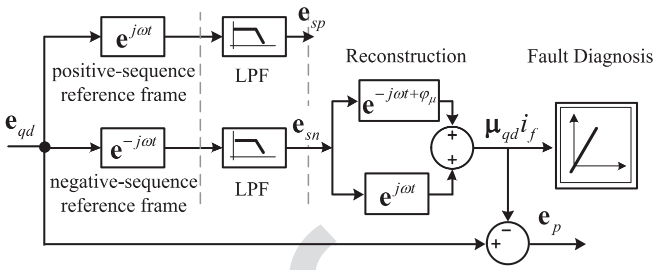

Fig. 4. Separation of sequence components of the RCV and decoupling of RCV-IF.

$$\widetilde{e}_{Ips} = \left(\frac{1}{Z} - \frac{1}{\hat{Z}}\right)\Delta_{vsp} + \frac{1}{3Z_f}\left\|\boldsymbol{\mu}_{qd}\right\|\widetilde{V}_{sp} \tag{24}$$

$$\widetilde{e}_{Isn} = \frac{1}{3Z_f}\boldsymbol{\mu}_{qd}\widetilde{V}_{sp}. \tag{25}$$

C. Decomposition of the RCV

The sequence decomposition of the RCV (block D-RCV in Fig. 3) is performed by employing the reference-frame theory [27], as shown in the detailed scheme of Fig. 4.

The signal processing of the RCV consist of three stages:

1) The resulting RCV signal in the *qd* stationary reference frame is referred to the positive-sequence synchronously rotating reference frame. In this new reference frame, the positive-sequence component must be a continuous signal and the negative-sequence component will be an oscillating signal. Simultaneously, the same process is performed to obtain the negative-sequence component by referring the RCV signal to the negative-sequence synchronously rotating reference frame.
2) The resulting signals are filtered through a LPF for separating each of the sequence components.

3) From the RCV-sequence components, the current error due to the interturn short-circuit fault, hereinafter called RCV-IF, given by $\boldsymbol{\mu}_{qd} i_f = [\mu_q i_f \; \mu_d i_f]^{\mathrm{T}}$, is reconstructed and is then isolated from the error produced by parameter variations and other disturbances $\mathbf{e}_p$. By continuing with the analysis, from (24) and (25) it can be seen that both components are proportional to the number of shorted turns $\left\|\boldsymbol{\mu}_{qd}\right\|$, and the fault current given by $\widetilde{I}_f = \frac{\widetilde{V}_{sp}}{Z_f}$. However, the positive-sequence component contains only the fault severity magnitude, [second term, $\left\|\boldsymbol{\mu}_{qd}\right\|$, in (24)], but it does not provide information about the location of the interturn fault in the phase windings. On the other hand, information about the stator fault phase/location is given in the angle of the negative-sequence component of the RCV, $(\angle\boldsymbol{\mu}_{qd} i_f)$. Therefore, in this paper, the location of the stator winding fault is obtained through difference between the relative positions of the sequence reference frames as follows:

$$\varphi_{\boldsymbol{\mu}} = \varphi_{e_{Isn}} - \varphi_{e_{Isp}} \tag{26}$$

where $\varphi_{e_{\mathrm{Ins}}}$ and $\varphi_{e_{Ips}}$ are the relative angles of the negative- and positive-sequence reference frame, respectively, with respect to the stationary reference frame. Finally, from the components (24)−(26), the RCV-IF is reconstructed and is then isolated from other disturbances, as shown in Fig. 4.

D. Detection and Isolation of Stator Fault

For the correct detection and quantification of the stator fault, it is necessary to propose reliable indicators. Based on the analysis in Section III-C, a fault severity factor (FSF) is defined as follows:

$$\mathrm{FSF} = \frac{\left\|\boldsymbol{\mu}_{qd} i_f\right\|}{I_{\mathrm{rms}}} \tag{27}$$

where I_{rms} is the rms value of the measured stator current.

For a healthy PMSM, FSF should be usually zero or close to zero. However, as mentioned above, several disturbances can cause that FSF become nonzero and false alarms could be triggered. Therefore, a threshold is defined for a healthy PMSM

$$J_{\mathrm{TH}} = \max_{\text{no fault}} \mathrm{FSF}. \tag{28}$$

The stator fault is detected if FSF $> J_{\mathrm{TH}}$ [29].

On the other hand, if the parameters error is neglected, the angle $\varphi_{\boldsymbol{\mu}}$ [in (26)] will assume the possible directions 0, $\frac{2\pi}{3}$, or $\frac{4\pi}{3}$, corresponding to phase a, b, or c, respectively. However, the first term related to the parameters error in (24) causes a slight angular rotation with respect to the ideal case that should be considered for a correct diagnosis. Therefore, considering the effect of undesirable disturbances, the complete isolation of the interturn fault in the stator windings is performed when the actual direction of RCV-IF $\varphi_{\boldsymbol{\mu}+}$ stay within the limits of the

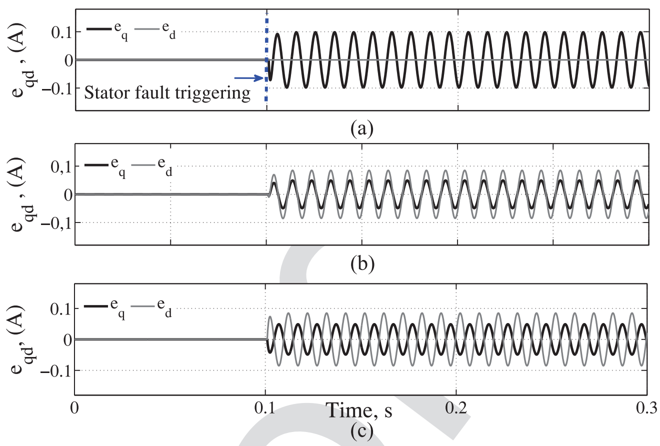

Fig. 5. RCV produced only by an interturn short-circuit fault in: (a) phase a. (b) phase b and (c) phase c.

"Fault Zone" in q-d plane, defined as

$$\boldsymbol{\mu}_{qd} i_{f_+} \equiv \begin{cases} \left\|\boldsymbol{\mu}_{qd} i_f\right\| \angle\varphi_{\mu+} & \text{for } -\frac{\pi}{6} + \varphi_\mu < \varphi_{\mu+} < \frac{\pi}{6} + \varphi_\mu \\ 0, & \text{other} \end{cases} \tag{29}$$

where $\varphi_{\mu+}$ is the actual direction of RCV-IF.

IV. Simulation of the Proposed Strategy

Simulation results of the proposed strategy were obtained using the PMSM model with stator fault presented in Section II-A. To evaluate the performance of the proposed method, a PMSM generator operating at different speed with a symmetrical three-phase resistance load connected is simulated. Thus, in this condition, a 2.6-A/100-Hz current is circulating into stator windings. Fig. 5 shows the RCV obtained from the difference between output currents by the proposed extended PMSM dynamic model with stator fault and the state observer based on a normal-operation PMSM model. Fig. 5(a) shows the RCV for a $\left\|\boldsymbol{\mu}_{qd}\right\| = 0.037$ (3.7% short circuit) fault severity produced in phase winding a. A similar fault, but in the phase winding b and c are shown in Fig. 5(b) and (c), respectively. In case that the current error is caused only by the stator fault (RCV-IF), the reconstructed signal $\boldsymbol{\mu}_{qd} i_f$ is exactly equal to RCV.

To evaluate the robustness of the proposed method, a series of tests including various disturbances were performed. Fig. 6 shows the results obtained by assuming: i) $+30\,\%$ variation of r_s, and ii) asymmetric load, which produces a $3\%\ \widetilde{I}_{ns}/\widetilde{I}_{ps}$ current unbalance. The RCV that includes the effects of all disturbances when at 0.1 s an interturn short-circuit fault is triggered, as shown Fig. 6(a). It can be seen that this RCV is not suitable for the stator fault detection. However, once the signal processing of RCV is performed (see Section III-C), the RCV-IF is shown in Fig. 6(b). This reconstructed signal accurately characterizes the interturn fault in PMSM $(\left\|\boldsymbol{\mu}_{qd} i_f\right\|, \angle\boldsymbol{\mu}_{qd} i_f)$. Due to the delay introduced by the LPF, the required time for the fault detection and isolation is approximately 30 ms. Finally, results from Fig. 6(c) show the RCV without the RCV-IF. According

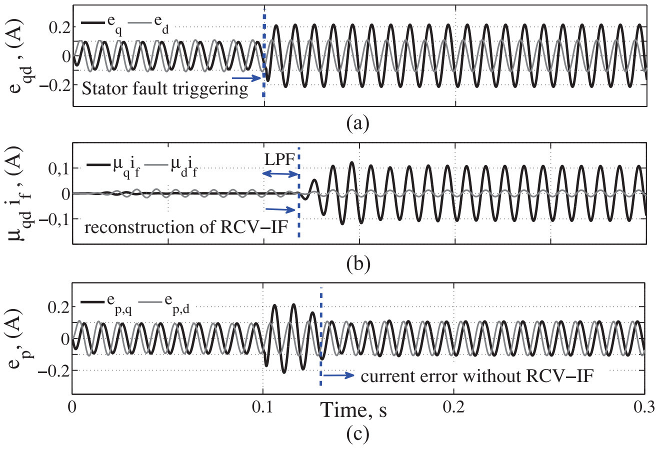

Fig. 6. (a) RCV including stator fault and other disturbances. (b) RCV-IF. (c) RCV without stator fault $\mathbf{e}_p$.

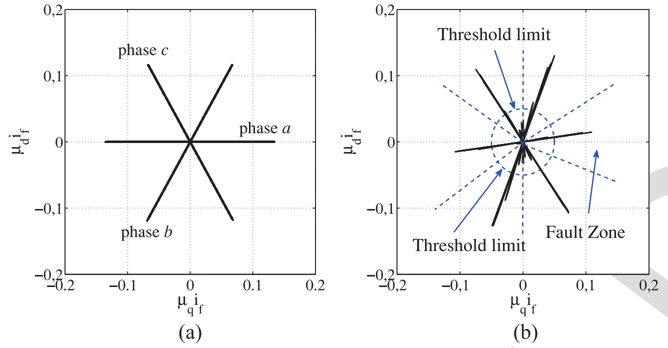

Fig. 7. RCV-IF indicating ten interturn short-circuit fault in *q*-*d* plane. (a) Ideal case. (b) Under parameter errors and unbalanced currents.

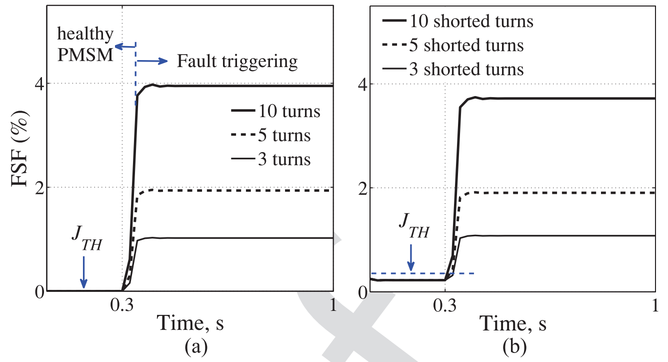

Fig. 8. FSF for several interturn short-circuit fault condition for 100% of rated load at 1500 r/min. (a) Ideal case, (b) Under parameter errors and unbalanced currents.

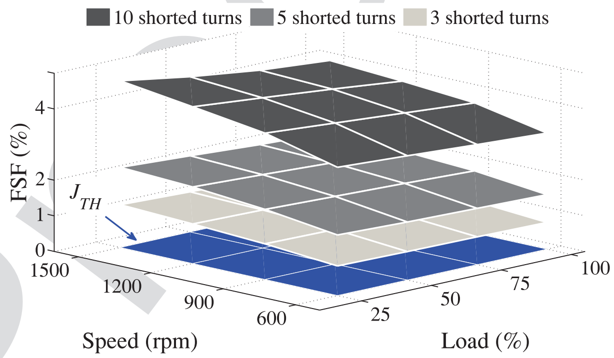

Fig. 9. FSF for different rotor speeds and loads.

TABLE I
PMSM PARAMETERS

Characteristic	Symbol	Value
Rated power (HP)	P_N	3/4
Rated volage (V)	V_N	300
Rated current (A)	I_N	2.7
Rated speed (r/min)	ω_r	2000
Number of pole pairs	P	4
Permanent magnet flux (Wb)	ψ_{pm}	0.17
Stator resistance (Ω)	r_s	3.15
Stator inductance (H)	L	$20e^{-3}$
Connection windings		Series
Turns/coil		30
Turns/phase		270

to the analysis of Section III-B, the resulting positive-sequence current error corresponds to $\widetilde{e}_{Ips}$ component [see (24) without the positive-sequence component of stator fault]. On the other hand, in order to determinate the vector angle φ_μ, the RCV-IF components shown in Fig. 5(a)–(c) can be represented in *q*-*d* plane as shown in Fig. 7(a). In this figure, the angular rotation of RCV-IF indicating the faulty phase winding can be clearly appreciated. Also, Fig. 7(b) shows the effects over the RCV-IF caused by disturbances considered in *i*) and *ii*). As mentioned above, the undesired disturbances cause a slight angular rotation with respect to the ideal case presented in Fig. 7(a). Therefore, the threshold limit and “Fault Zone” in *q*-*d* plane is defined for guaranteeing the reliability of the interturn fault isolation (see Section III-D).

The performance of FSF for different stator fault conditions is shown in Fig. 8. Fig. 8(a) shows the FSF for 3, 5, and 10 shorted turns with balanced load currents. In this ideal case, the threshold could be defined as $J_{\rm TH} = 0$. On the other hand, Fig. 8(b) shows the FSF for ten shorted turns with parameter errors and unbalanced currents [see conditions i) and ii)]. In these cases, the threshold must be defined as $J_{\rm TH} \neq 0$, and fault detection is performed when FSF $> J_{\rm TH}$. However, the estimated fault severity is correctly indicated for all the evaluated cases. Fig. 9 shows the performance of FSF for different angular speed and load conditions. Note that FSF increases with the number of shorted turns, but it is not very sensitive to the angular speed and the load condition of the PMSM. These characteristics of the FSF can be justified on the flat and equidistant surfaces obtained for 3, 5, and 10 shorted turns.

V. EXPERIMENTAL VALIDATION

To validate the proposed model-based method, several experimental tests were performed using a 3/4 HP PMSM whose parameters are shown in Table I. This three-phase PMSM prototype with modified stator allows adjusting the fault severity from the first, third, fifth, and tenth turns of one coil of the phase

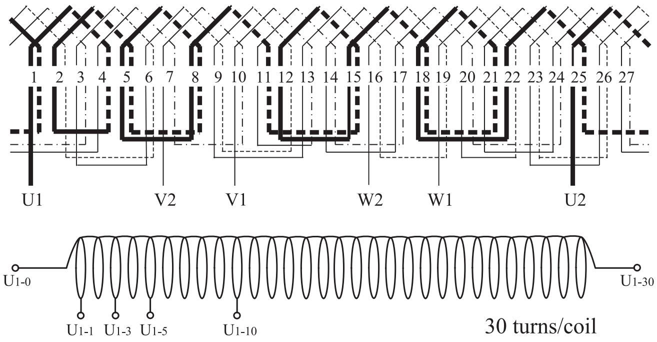

Fig. 10. Modified stator winding with additional connections.

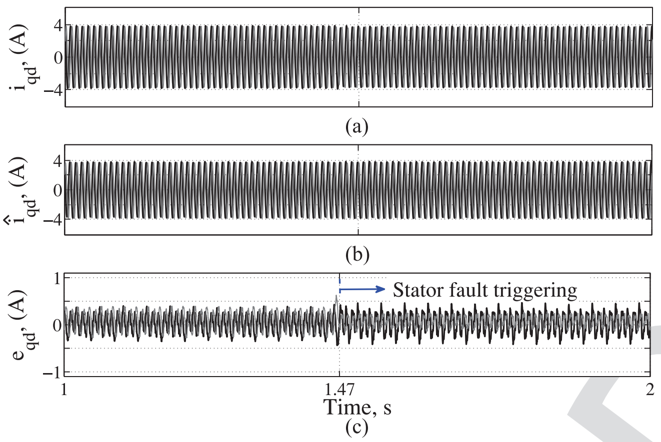

Fig. 11. Ten turns short-circuit fault in phase winding *c*. (a) Measured currents. (b) Estimated currents. (c) RCV.

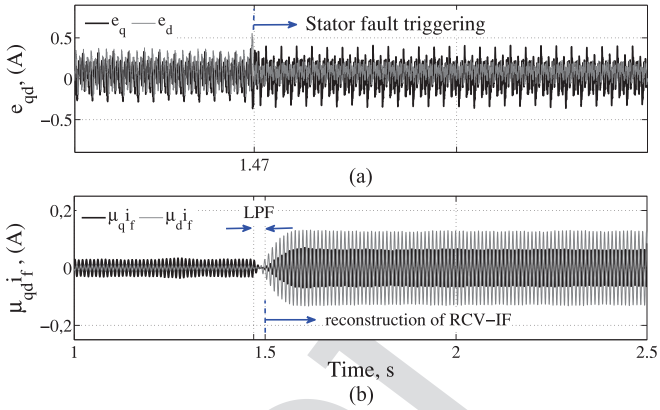

Fig. 12. Faulty PMSM. (a) RCV including ten interturn short-circuit fault in phase winding *c*. (b) RCV-IF decoupled.

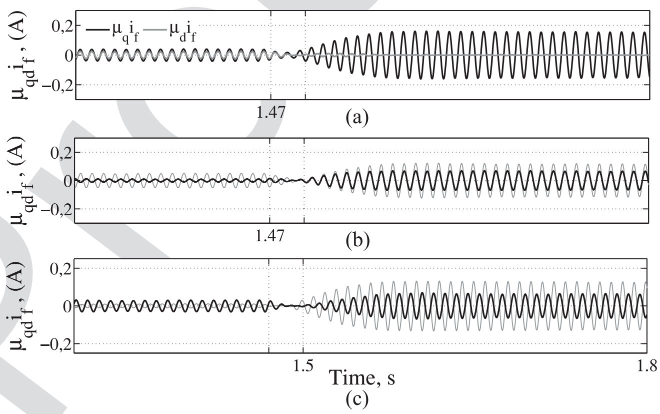

Fig. 13. Reconstruction of the RCV-IF with ten interturn short-circuit fault in (a) phase *a*, (b) phase *b* and, (c) phase *c*.

winding (0.37% to 3.7 turns with respect to the total turns of the complete phase winding). Fig. 10 shows a scheme of stator winding distribution of the PMSM (top picture). A detail of the additional connections from the first, third, fifth, and tenth turns of one coils of the winding phase is shown in the same figure (bottom picture). The test bench developed and built for experimental validation is composed by a voltage-source power electronic converter to continuously control the speed of a three-phase IM. The shaft of the IM is directly coupled to the PMSM, similar to the *Direct-Drive* generator technology in wind energy conversion systems. In this configuration, a three-phase resistance load $r_{abc} = 23.6\,\Omega$ is connected to the terminals of the PMSM in order to obtain the nominal output current. Furthermore, in order to safeguard the stator windings of high fault-currents, the experimental tests were performed for a short time (approx. 4 s), and by also connecting an external resistor between the terminals of the shorted turns $r_f = 149$ mΩ. On the other hand, an oscillographic recorder at a sampling frequency of $f_s = 8$ kS/s was used to measure and record two stator current using Current Clamp Probes Fluke i200s and two line voltages using Differential Voltage Probes Agilent N2772 A.

Fig. 11 shows the performance of *q-d* stator current when ten turns (3.7% short circuit) is intentionally produced at approximately 1.5 s. For this fault severity condition, the measured stator currents ($\widetilde{I}_{sp} = 2.7$ A rms) for the PMSM at 1500 r/min are shown in Fig. 11(a). On the other hand, Fig. 11(b) shows the stator currents estimated by using the state observer. The RCV obtained is shown in Fig. 11(c). Fig. 12 shows the result of signal processing of the RCV. In Fig. 12(a), a current error without stator fault (before of 1.5 s) can be appreciated due to various asymmetries such as differences between parameter values of the state observer and the PMSM rated parameters, load unbalance, or potential inherent asymmetries, among others. Such disturbances produce an inherent unbalance of stator currents of 0.5% $\widetilde{I}_{ns}/\widetilde{I}_{ps}$. Therefore, in order to avoid false alarms, a threshold limit is set for the healthy PMSM condition (see Section III-D). From this threshold limit preset, the proposed method allows the correct detection and isolation of the RCV-IF from any other perturbations, as shown in Fig. 12(b). Note that the LPF delays the detection of the fault by about 30 ms approximately, similar to Fig. 6. Fig. 13 shows the reconstructed fault vector, RCV-IF, for each faulty phase winding. By analyzing these results, it can be seen that RCV-IF significantly differs according to the location of the interturn short-circuit fault into the phase winding *a*, *b*, or *c*, respectively. On the other hand, the RCV-IF represented in *q-d* plane for each faulty phase winding is shown in Fig. 14. In these figures, the threshold set $J_{\rm TH}$ for detection of a stator fault without errors is presented (circle in dashed lines). It can be clearly seen that a stator fault

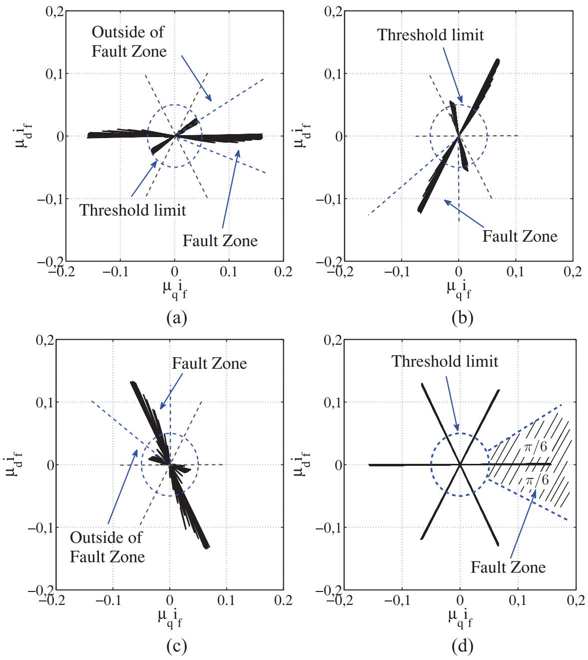

Fig. 14. RCV-IF indicating ten interturn short-circuit fault in (a) phase *a*, (b) phase *b*, (c) phase *c*, and (d) all cases superposed.

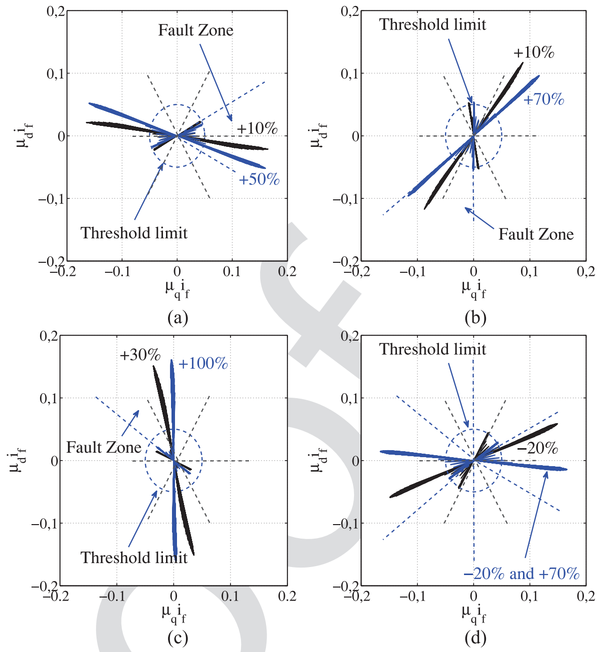

Fig. 15. RCV-IF with parametric variations on (a) phase *a*, (b) phase *b*, (c) phase *c*, (d) simultaneous parametric variations on phase *a*.

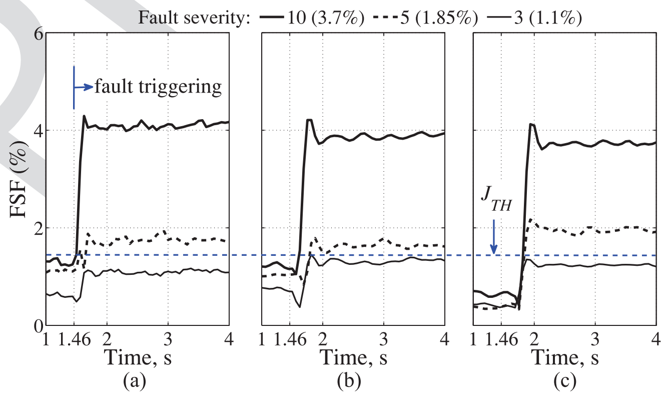

Fig. 16. FSF for several interturn short-circuit fault conditions for 100% of rated load: (a) 1500 r/min, (b) 1200 r/min, and (c) 900 r/min.

(10 shorted turns) is detected once the fault severity exceed the preset threshold limit. It is important to note that the magnitude of the fault severity is the same regardless of the faulty phase winding, but the direction of RCV-IF in *q*-*d* plane changes indicating the location of the stator fault on the machine windings. In order to improve the visualization of the defined "Fault Zone" [see (29)], all the analyzed cases starting from the triggered fault (since 1.5 s) are superposed and shown in Fig. 14(d). In this figure, for a correct detection and isolation of a stator fault in winding phase *a*, the region in the *q*-*d* plane greater than the threshold limit set J_{TH} and also delimited by two rays forming a $\frac{\pi}{3}$ rad. angle (marked in dashed lines). Due to the threshold limit set for prevent false alarms for the healthy PMSM condition, it is difficult to detect short circuits below five turns, depending on the value of the fault current. However, the magnitude of the fault current is less important for small amounts of shorted turns, similar to the magnitude of the rated current. In these cases, the operating conditions such as stator winding temperature and the degree of current unbalance are similar to PMSM normal-operating conditions. When stator fault involves a considerable amounts turns, the fault current and the temperature of the affected winding portion become important, but the detection is ensured as soon as the threshold is exceeded.

With the goal of evaluating the robustness of the proposed method, several experimental tests were performed considering different perturbations and transient conditions.

1) *Parametric Variations:* Fig. 15 shows the RCV-IF under the effects of the introduced disturbances.

a) +10% and +50% of r_s on phase *a*, Fig. 15(a);
b) +10% and +70% of r_s on phase *b*, Fig. 15(b);
c) +30% and +100% of r_s on phase *c*, Fig. 15(c);
d) −20% of L and simultaneous variations of: +70% of r_s and also −20% of L, Fig. 15(d).

As mentioned in Section III-C, the effects of resistances and inductances variations cause a rotation of RCV-IF in *q*-*d* plane due to the change of nominal characteristic impedance $\hat{Z}$.

Therefore, if simultaneous parametric variations were produced, RCV draws a geometric arc in *q*-*d* plane whose radius will be equal to the fault severity. Note that the correct fault diagnosis is completely guaranteed while RCV-IF direction is located within the limits of the Fault Zone. In all the cases analyzed so far, the estimated magnitude of the fault severity is invariant to the faulty phase winding and the effects introduced by various asymmetries.

2) *Different Operating Conditions (Speed and Load):* The performance of the FSF for different operating speeds at rated load obtained for 3, 5, and 10 shorted turns is shown in Fig. 16. In all cases, fault detection is performed once the J_{TH} is exceeded. Similar to Fig. 8(a), FSF indicates practically the same fault

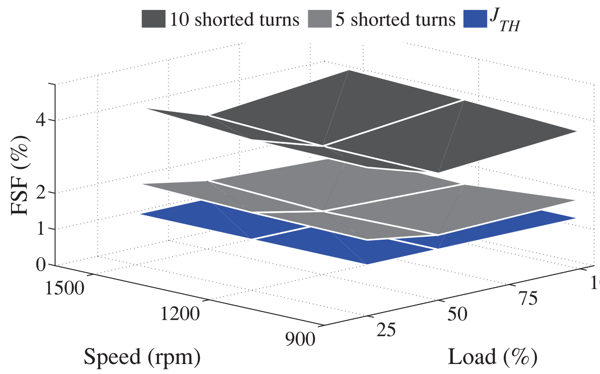

Fig. 17. FSF for several interturn short-circuit fault conditions and different rotor speeds and loads.

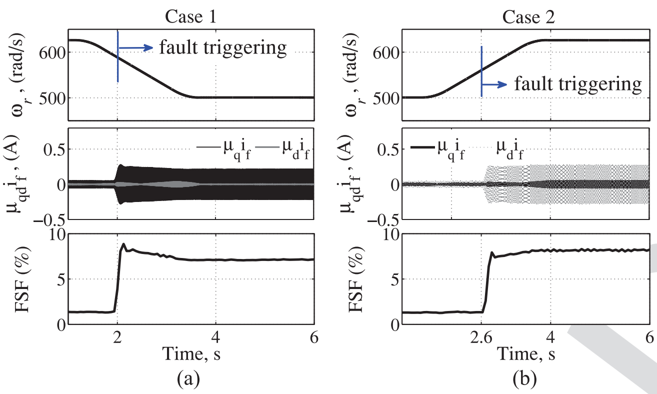

Fig. 18. FSF for transient condition. (a) Case 1: interturn short-circuit fault in phase *a*. (b) Case 2: interturn short-circuit fault in phase *c*.

severity regardless of the angular speed of the PMSM. Fig. 17 shows the FSF for different rotor speed and load conditions. The flat and equidistant surfaces obtained are similar to the simulation results shown in Fig. 9. Thus, severity of the fault is also determined with good accuracy for various operating conditions.

3) *Transient Conditions:* The performance of the proposed method for the PMSM under transient conditions is shown in Fig. 18. Case 1 shows an interturn short circuit on phase *a*. Stator fault is triggered during a speed transient with a descendant ramp. Case 2 shows a interturn short-circuit on phase *c*. In this case, stator fault is triggered during a speed transient with an ascendant ramp. Fig. 18 (top picture) shows the angular speed obtained from (12). RCV-IF for the transient conditions are represented in the same figure (middle picture). Note that the RCV-IF for cases 1 and 2 are analogous to the results shown in Fig. 13(a) and (c), respectively. Ultimately, FSF (bottom picture) present similar behavior to the results in Fig. 16. In all the evaluated cases, the LPF delays the fault detection with times similar to those shown in Figs. 6 and 12. Finally, it is important to note that the sensitivity of the proposed method in front of non-modeled irregularities, measurement asymmetries, or parametric variations are analogous to the sensitivity of other previous methods based on analysis of current error from the measurement of electric variables [16], [18], [23], [25], [29].

VI. Conclusion

A new model-based method for interturn short-circuit fault detection and isolation in permanent magnet synchronous machines was proposed in this paper. This method only requires the currents and voltages measurement at terminals of the PMSM, and thus, it may be implemented online without the need of an additional position or speed sensor for knowing the rotor speed. An extended PMSM dynamic model including an interturn short-circuit fault in any phase stator-windings was presented. From this model, the PMSM steady-state sequence component models were derived in order to analyze its behavior under stator faults. Additionally, a state observer based on a normal-operation model of the PMSM was proposed to estimate stator currents. Incipient stator fault detection and isolation was performed through the RCV-IF signal generated by the difference between the measured and estimated stator currents.

From the results of experimental tests obtained by using a PMSM prototype, we demonstrated that it is possible to detect and isolate a 1.85% interturn short-circuit fault in any phase-windings. Since model inexactitudes or parameter uncertainties affect the performance of model-based methods, the robustness and reliability were analyzed by introducing asymmetric currents and variations of parameters of the state observer. Simulations and experimental test results obtained for the PMSM at different operation points allowed us to evaluate the accuracy and effectiveness of the method proposed. Due to the impact of the disturbances over the RCV, a FSF and also a Fault Zone in *q*-*d* plane were defined in order to set alarm levels to ensure the minimum detectable amount of shorted turns and to locate correctly the stator fault in the windings.

References

[1] P. Sekerak, V. Hrabovcova, J. Pyrhonen, S. Kalamen, P. Rafajdus, and M. Onufer, "Comparison of synchronous motors with different permanent magnet and winding types," *IEEE Trans. Magn.*, vol. 49, no. 3, pp. 1256–1263, Mar. 2013.

[2] S. Grubic, J. M. Aller, L. Bin, and T. G. Habetler, "A survey on testing and monitoring methods for stator insulation systems of low-voltage induction machines focusing on turn insulation problems," *IEEE Trans. Ind. Electron.*, vol. 55, no. 12, pp. 4127–4136, Dec. 2008.

[3] A. Bellini, F. Filippetti, C. Tassoni, and G. A. Capolino, "Advances in diagnostic techniques for induction machines," *IEEE Trans. Ind. Electron.*, vol. 55, no. 12, pp. 4109–4126, Dec. 2008.

[4] S. Moon, J. Lee, H. Jeong, and S. W. Kim, "Demagnetization fault diagnosis of a PMSM based on structure analysis of motor inductance," *IEEE Trans. Ind. Electron.*, vol. 63, no. 6, pp. 3795–3803, Jun. 2016.

[5] H. Hashemian, "State-of-the-art predictive maintenance techniques," *IEEE Trans. Instrum. Meas.*, vol. 60, no. 1, pp. 226–236, Jan. 2011.

[6] K.-H. Kim, "Simple online fault detecting scheme for short-circuited turn in a PMSM through current harmonic monitoring," *IEEE Trans. Ind. Electron.*, vol. 58, no. 6, pp. 2565–2568, Jun. 2011.

[7] R. Z. Haddad and E. G. Strangas, "On the accuracy of fault detection and separation in permanent magnet synchronous machines using MCSA/MVSA and LDA," *IEEE Trans. Energy Convers.*, vol. 31, no. 3, pp. 924–934, Sep. 2016.

[8] Y. Duan and H. Toliyat, "A review of condition monitoring and fault diagnosis for permanent magnet machines," in *Proc. IEEE Power Energy Soc. Gen. Meeting*, 2012, pp. 1–4.

[9] J. Hang, J. Zhang, M. Cheng, and J. Huang, "Online interturn fault diagnosis of permanent magnet synchronous machine using zero sequence components," *IEEE Trans. Power Electron.*, vol. 30, no. 12, pp. 6731–6741, Dec. 2015.

[10] E. Strangas, S. Aviyente, and S. Zaidi, “Frequency analysis for efficient fault diagnosis and failure prognosis for interior permanent-magnet AC motors,” *IEEE Trans. Ind. Electron.*, vol. 55, no. 12, pp. 4191–4199, Dec. 2008.

[11] S. Watson, B. Xiang, W. Yang, P. Tavner, and C. Crabtree, “Condition monitoring of the power output of wind turbine generators using Wavelets,” *IEEE Trans. Energy Convers.*, vol. 25, no. 3, pp. 715–721, Sep. 2010.

[12] J. Rosero, L. Romeral, J. Ortega, and E. Rosero, “Short-circuit detection by means of empirical mode decomposition and Wigner–Ville distribution for PMSM running under dynamic condition,” *IEEE Trans. Ind. Electron.*, vol. 56, no. 11, pp. 4534–4547, Nov. 2009.

[13] B. Aubert, J. Régnier, S. Caux, and D. Alejo, “Kalman-filter-based indicator for online interturn short circuits detection in permanent-magnet synchronous generators,” *IEEE Trans. Ind. Electron.*, vol. 62, no. 3, pp. 1921–1930, Mar. 2015.

[14] S. Nadarajan, S. K. Panda, B. Bhangu, and A. K. Gupta, “Online model-based condition monitoring for brushless wound-field synchronous generator to detect and diagnose stator windings turn-to-turn shorts using extended Kalman filter,” *IEEE Trans. Ind. Electron.*, vol. 63, no. 5, pp. 3228–3241, May 2016.

[15] R. Isermann, *Fault-Diagnosis Applications*, 1st ed. New York, NY, USA: Springer-Verlag, 2011.

[16] C. H. De Angelo, G. R. Bossio, S. J. Giaccone, M. I. Valla, J. A. Solsona, and G. O. Garcia, “Online model-based stator-fault detection and identification in induction motors,” *IEEE Trans. Ind. Electron.*, vol. 56, no. 11, pp. 4671–4680, Nov. 2009.

[17] L. Romeral, J. C. Urresty, J. R. Riba Ruiz, and A. Garcia Espinosa, “Modeling of surface-mounted permanent magnet synchronous motors with stator winding interturn faults,” *IEEE Trans. Ind. Electron.*, vol. 58, no. 5, pp. 1576–1585, May 2011.

[18] I. Jeong, B. J. Hyon, and K. Nam, “Dynamic modeling and control for SPMSMs with internal turn short fault,” *IEEE Trans. Power Electron.*, vol. 28, no. 7, pp. 3495–3508, Jul. 2013.

[19] B. G. Gu, “Study of IPMSM interturn faults—Part I: Development and analysis of models with series and parallel winding connections,” *IEEE Trans. Power Electron.*, vol. 31, no. 8, pp. 5931–5943, Aug. 2016.

[20] N. H. Obeid, T. Boileau, and B. Nahid-Mobarakeh, “Modeling and diagnostic of incipient interturn faults for a three-phase permanent magnet synchronous motor,” *IEEE Trans. Ind. Appl.*, vol. 52, no. 5, pp. 4426–4434, Sep./Oct. 2016.

[21] R. M. Tallam, T. G. Habetler, and R. G. Harley, “Transient model for induction machines with stator winding turn faults,” *IEEE Trans. Ind. Appl.*, vol. 38, no. 3, pp. 632–637, May/Jun. 2002.

[22] N. Leboeuf, T. Boileau, B. Nahid-Mobarakeh, N. Takorabet, F. Meibody-Tabar, and G. Clerc, “Effects of imperfect manufacturing process on electromagnetic performance and online interturn fault detection in PMSMs,” *IEEE Trans. Ind. Electron.*, vol. 62, no. 6, pp. 3388–3398, Jun. 2015.

[23] A. Sarikhani and O. A. Mohammed, “Inter-turn fault detection in PM synchronous machines by physics-based back electromotive force estimation,” *IEEE Trans. Ind. Electron.*, vol. 60, no. 8, pp. 3472–3484, Aug. 2013.

[24] N. H. Obeid, T. Boileau, and B. Nahid-Mobarakeh, “Modeling and diagnostic of incipient inter-turn faults for a three phase permanent magnet synchronous motor using Wavelet transform,” in *Proc. IEEE Ind. Appl. Soc. Annu. Meeting*, Oct. 2015, pp. 1–8.

[25] N. Leboeuf, T. Boileau, B. Nahid-Mobarakeh, G. Clerc, and F. Meibody-Tabar, “Real-time detection of interturn faults in PM drives using back-EMF estimation and residual analysis,” *IEEE Trans. Ind. Appl.*, vol. 47, no. 6, pp. 2402–2412, Nov. 2011.

[26] M. A. Mazzoletti, G. R. Bossio, C. H. De Angelo, and D. R. Espinoza-Trejo, “Analysis and validation of a dynamic model for PMSM with stator fault,” in *Proc. XVI Reunión Trabajo en Procesamiento Información Control*, Oct. 2015, pp. 1–6.

[27] P. Krause, O. Wasynczuk, S. Sudhoff, and S. Pekarek, *Analysis of Electric Machinery and Drive Systems*, 3rd ed. Piscataway, NJ, USA: IEEE Press, 2013.

[28] A. Dabroom and H. K. Khalil, “Numerical differentiation using high-gain observers,” in *Proc. 36th IEEE Conf. Decision Control*, vol. 5, Dec. 1997, pp. 4790–4795.

[29] D. R. Espinoza-Trejo, D. Campos-Delgado, G. R. Bossio, E. Bárcenas, J. Hernández-Díez, and L. Lugo-Cordero, “Fault diagnosis scheme for open-circuit faults in field-oriented control induction motor drives,” *IET Power Electron.*, vol. 6, no. 5, pp. 869–877, May 2013.

Manuel A. Mazzoletti (S’12) received the Electronic Engineering degree from the Universidad Nacional de Misiones, Posadas, Argentina, in 2006, and the Doctor of Engineering degree from the Universidad Nacional de Río Cuarto, Río Cuarto, Argentina, in 2017.

Since 2012, he has been with the Grupo de Electrónica Aplicada, Facultad de Ingeniería, Universidad Nacional de Río Cuarto. He is also currently with the Consejo Nacional de Investigaciones Científicas y Técnicas, Argentina. His research interests include fault diagnosis of electric machines, ac motor drives, and renewable energy generation.

Guillermo R. Bossio (S’03–M’07–SM’15) received the Electrical Engineering degree from the Universidad Nacional de Río Cuarto, Río Cuarto, Argentina, in 1999, and the Doctor of Engineering degree from the Universidad Nacional de La Plata, Buenos Aires, Argentina, in 2004.

Since 1994, he has been with the Grupo de Electrónica Aplicada, Facultad de Ingeniería, Universidad Nacional de Río Cuarto. He is also currently with the Consejo Nacional de Investigaciones Científicas y Técnicas, Argentina. His research interests include fault diagnosis of electric machines, ac motor drives, electric vehicles, and renewable energy generation.

Cristian H. De Angelo (S’96–M’05–SM’10) received the Electrical Engineering degree from the Universidad Nacional de Río Cuarto, Río Cuarto, Argentina, in 1999, and the Doctor of Engineering degree from the Universidad Nacional de La Plata, Ensenada, Argentina, in 2004.

In 1994, he joined the Grupo de Electrónica Aplicada, Universidad Nacional de Río Cuarto. He is currently an Associate Professor at the Universidad Nacional de Río Cuarto and an Independent Researcher with the Consejo Nacional de Investigaciones Científicas y Técnicas, Buenos Aires, Argentina. His research interests include electric and hybrid vehicles, fault diagnosis of electric machines, electric motor control, and renewable energy generation.

Diego R. Espinoza-Trejo (A’10) was born in San Luis Potosí, México. He received the B.S. degree in electronics engineering and the M.Sc. and Ph.D. degrees in electrical engineering from the Universidad Autónoma de San Luis Potosí, San Luis Potosí, in 2001, 2004, and 2008, respectively.

In 2009, he joined the Mechatronics Department, Coordinación Académica Región Altiplano, Universidad Autónoma de San Luis Potosí. He is currently a Professor at the Universidad Autónoma de San Luis Potosí and a Researcher with the Consejo Nacional de Ciencia y Tecnología, México. His main research interests include active fault-tolerant control and fault diagnosis of power electronic systems, fault diagnosis of electric machines, and photovoltaic systems.